

1 **Anisotropic physical properties of U_2Rh_2Sn single crystal in high**
2 **magnetic fields**

3 K. Prokeš,^{1,*} D. I. Gorbunov,² M. Reehuis,¹ B. Klemke,¹ A. Gukasov,³ K. Uhlířová,⁴
4 X. Fabrèges,³ Y. Skourski,⁵ F. Yokaichiya,¹ S. Hartwig,¹ and A.V. Andreev⁶

5 ¹*Helmholtz-Zentrum Berlin für Materialien und Energie, 14109 Berlin, Germany*

6 ²*Dresden High Magnetic Field Laboratory (HLD-EMFL),*
7 *Helmholtz-Zentrum Dresden-Rossendorf, 01314 Dresden, Germany*

8 ³*Laboratoire Léon Brillouin, CEA, CNRS, Université Paris-Saclay,*
9 *CEA-Saclay, 91191 Gif-sur-Yvette, France*

10 ⁴*Faculty of Mathematics and Physics,*
11 *Charles University, 121 16 Praha 2, The Czech Republic*

12 ⁵*Dresden High Magnetic Field Laboratory (HLD-EMFL),*
13 *Helmholtz-Zentrum Dresden-Rossendorf, D-01314 Dresden, Germany*

14 ⁶*Institute of Physics, Academy of Sciences of the*
15 *Czech Republic, 182 21 Prague, Czech Republic*

16 (Dated: March 8, 2017)

Abstract

We report on the crystal and magnetic structures, magnetic, transport and thermal properties of $\text{U}_2\text{Rh}_2\text{Sn}$ single crystals studied in part in high magnetic fields up to 58 T. The material adopts a U_3Si_2 -related tetragonal crystal structure and orders antiferromagnetically below $T_N = 25$ K. The antiferromagnetic structure is characterized by a propagation vector $\mathbf{k} = (0\ 0\ \frac{1}{2})$. The magnetism in $\text{U}_2\text{Rh}_2\text{Sn}$ is found to be associated mainly with $5f$ states. However, both unpolarized and polarized neutron experiments reveal at low temperatures in zero field non-negligible magnetic moments also on Rh sites. U moments of $0.50(2)\ \mu_B$ are directed along the tetragonal axis while and Rh moments of $0.06(4)\ \mu_B$ form a non-collinear arrangement confined to the basal plane. The response to applied magnetic field is highly anisotropic. Above ~ 15 K the easy magnetization direction is along the tetragonal axis. At lower temperatures, however, a stronger response is found perpendicular to the c axis. While for the a axis no magnetic phase transition is observed up to 58 T, for the field applied at 1.8 K along the tetragonal axis we observe above 22.5 T a field-polarized state. A magnetic phase diagram for the field applied along the c axis is presented.

¹⁷ PACS numbers: 75.25.-j, 75.30.-m

18 I. INTRODUCTION

19 Uranium based compounds are harboring a plethora of various physical properties and
20 ground states that range from paramagnetism through spin fluctuations and heavy-fermionic
21 states towards a long-range ferromagnetic or antiferromagnetic (AF) order¹. In these mate-
22 rials superconductivity may coexist with a long-range magnetic order and exotic states like
23 hidden order in URu₂Si₂ can be realized as well²⁻⁴. All these materials show hybridization
24 effects of the uranium 5*f* electron states with the wave functions of the *s*, *p* and *d* wave
25 functions of the surrounding ligands and conduction electrons. As the strength of hybridiza-
26 tion depend not only on the geometry of the 5*f*-containing atoms and distances to their
27 neighbors but also on the type of ligands, studies on large groups of intermetallic compounds
28 crystallizing in the same crystal structure play an important role in determining the gen-
29 eral trends of the interplay between the direct 5*f*-5*f* overlap of electron wave functions,
30 5*f*-ligand hybridization and the resulting ground states¹. Intermetallic compounds with a
31 U₃Si₂-type structure constitute such a large group of compounds⁵⁻¹⁰. U₂Rh₂Sn adopts this
32 structure which consists from two alternating planes, one containing only uranium atoms
33 and the other Rh and Sn atoms. Projections along the *a* axis and the *c* axis are shown in
34 Fig. 1(a) and (b), respectively.

35 In most uranium compounds U magnetic moments orient within a plane perpendicular
36 to the shortest U-U links^{9,10}. The generally accepted explanation is the increase of charge
37 density in the U-U direction due to the direct 5*f*-5*f* wavefunction overlap, which simulta-
38 neously increases the density of orbital currents and causes moments perpendicular to these
39 directions⁹. However, some materials like U₂Rh₂Sn constitute an exemption to this simple
40 rule¹⁰. The shortest 5*f*-5*f* distance of $d_0 = 3.586 \text{ \AA}$ is found along the *c* axis. Each U atom
41 has two such nearest neighbors. The distances between U atoms within the basal plane are
42 larger: there is one next-nearest neighbor at a distance $d_1 = 3.622 \text{ \AA}$ and four second-next-
43 nearest neighbors at a distance $d_2 = 3.902 \text{ \AA}$. Despite the fact that $d_0 < d_1$ the moments
44 are reported to be directed along the shorter-distance direction^{9,11}. In Fig. 1(c) we show
45 the U atom sublattice with marked links and the equivalency of the U₂Rh₂Sn crystal struc-
46 ture with the Shastry-Sutherland lattice (SSL) (Fig. 1(d)) known to show magnetization
47 plateaus¹². Corresponding exchange interactions are denoted as J and J' , respectively. In
48 the SSL, magnetic moments orient perpendicular to the unique axis as the case of TbB₄¹³.

49 Although not shown in Fig. 1, $\text{U}_2\text{Rh}_2\text{Sn}$ Rh atoms form such a type of lattice as well.

50 $\text{U}_2\text{Rh}_2\text{Sn}$ has been subject of numerous studies that include crystal structure determination^{5,6},
51 dc and ac magnetic susceptibility^{5,11,14,15}, transport properties¹⁶, high-field magnetization^{7,8,17,18},
52 specific heat^{9,15} and neutron diffraction^{9,11,19}. Except for a study by Pereira et al.¹¹ that re-
53 ports low-field magnetic bulk properties and neutron diffraction of a $\text{U}_2\text{Rh}_2\text{Sn}$ single crystal,
54 all literature deals with polycrystalline samples. The magnetization process at high fields is
55 reported to be quite unusual. Firstly, different measurements using different pulse lengths
56 came to contradicting conclusions regarding the type of the magnetocrystalline anisotropy
57 and secondly, the magnetization process is by itself highly unusual as it shows strong hys-
58 teretic behavior not only around the transition but also in the wide field range above it, i.e.
59 in the polarized state.

60 The magnetic structure of $\text{U}_2\text{Rh}_2\text{Sn}$ is reported to be AF, characterized by a propagation
61 vector $\mathbf{k} = (0\ 0\ \frac{1}{2})^{9,11}$. Strongly reduced U moments of 0.38-0.53 μ_B are reported to be
62 directed along the c axis. However, both the powder and single-crystalline neutron diffraction
63 were inconclusive regarding the possible magnetic moment on Rh sites^{9,11}. This point is
64 important as it is not that uncommon that transition metal sites carry a substantial magnetic
65 moment as a result of $5f$ -ligand hybridization^{20,21}. This fact together with a remaining
66 controversy regarding the high-field magnetization process prompted us to re-investigate
67 this system.

68 Keeping in mind that a large magnetocrystalline anisotropy is present in this system, we
69 have prepared single-crystalline sample and performed a series of bulk measurements in low
70 and elevated magnetic fields applied along the principal axes. We report on magnetic bulk
71 properties, electrical resistivity, specific heat, unpolarized and polarized neutron diffraction
72 in fields up to 14.5 T and 6.2 T, respectively and high-field magnetization in high magnetic
73 fields up to 58 T leading to a construction of a magnetic phase diagram. Both, polarized
74 and unpolarized neutron diffraction experiments showed that non-negligible magnetic mo-
75 ments are associated with Rh sites oriented perpendicular to the c axis. This, in turn may
76 explain the unusual shape of the magnetization curve encountered above the metamagnetic
77 transition that takes place at ~ 22 T.

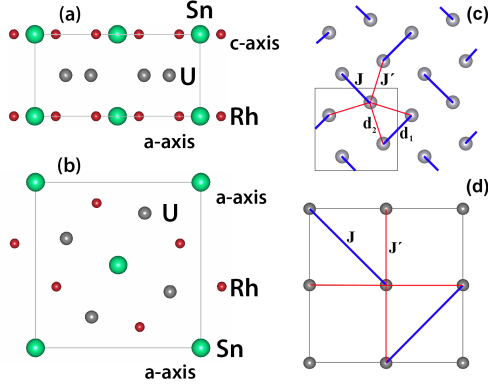


FIG. 1. (Color online) Crystal structure of U_2Rh_2Sn as determined from neutron data projected along the a axis (a) and the c axis (b). Sn, U and Rh atoms are shown by large, intermediate and small spheres, respectively. A sublattice formed by U atoms projected along the tetragonal axis is shown in (c). The thick (blue) lines connect the next-nearest uranium neighbors (at a distance $d_1 = 3.622 \text{ \AA}$) and the thin line (red) the second-next-nearest neighbors (at a distance $d_2 = 3.902 \text{ \AA}$). Corresponding exchange interactions are denoted as J and J' , respectively. The nearest U neighbors (at a distance $d_0 = 3.586 \text{ \AA}$) are found along the c axis. The rectangle represents one crystallographic unit cell projected along the c axis. U atoms form effectively a Shastry-Sutherland lattice as shown in (d). Rh atoms form this type of lattice as well.

79 II. EXPERIMENTAL

80 A large single crystal of U_2Rh_2Sn has been grown using a modified tri-arc Czochralski
 81 technique in an ultrapure argon atmosphere from a stoichiometric melt of the constituent
 82 elements, which were melted several times before the growing process to obtain a homo-
 83 geneous distribution of elements. The purity of used elements was Rh 99.95 %, Sn99.995
 84 % and U 99.5 %. Uranium was additionally purified by the Solid State Electrotransport
 85 method²².

86 The quality and homogeneity of the single crystal was determined using x-ray Laue
 87 diffraction and by scanning electron microscopy (SEM) equipped with a back scattered
 88 electron detector (BSE) and energy dispersive X-ray detector (EDX). The BSE contrast
 89 revealed presence of two types of well localized impurities (approx. 3 vol. %) in an
 90 otherwise homogeneous single crystal. According to EDX analysis, the majority phase has a
 91 composition $U_{2.07(14)}Rh_{1.96(7)}Sn_{0.97(7)}$. The spurious impurities are unknown U-rich ternary

92 phases with composition varying from $U_{3.3}Rh_2Sn$ to a phase containing 95 % of uranium.

93 The single crystal was oriented by the Laue method and cut by a spark-erosion saw along
94 the principal crystallographic axes. The top part of the ingot, pulverized under protective
95 atmosphere, was used to obtain X-ray powder diffraction data using an Cu K-alpha Bruker
96 powder diffractometer. The data were analyzed using a Rietveld type refinement with the
97 Jana2006 software²³.

98 Electrical resistivity, magnetization $M(T)$ and the static magnetic susceptibility $\chi =$
99 M/H , where H denotes the applied magnetic field, were measured between 2 and 300 K
100 using the Quantum Design 14 T Physical Properties Measurements System (PPMS). For the
101 magnetization measurements the vibrating sample magnetometer (VSM) option was used.
102 Resistivity measurements were performed using the standard four-point DC method.

103 Pulsed high magnetic field measurements have been performed at the High Field Lab-
104 oratory of the Helmholtz Zentrum Dresden-Rossendorf. We have used three small single
105 crystals with weight between 30 and 44 mg. Crystals were oriented along the [100], [110]
106 and [001] directions. The magnetization $M(H)$ measurements were performed between 1.8
107 K and 30 K in fields up to 58 T generated by discharging a capacitor bank producing 25
108 ms long magnetic field pulse. For the c axis direction we have collected data also at 640
109 mK achieved using a 3He refrigerator. In this case, in order to minimize heating by eddy
110 currents, we have utilized a longer pulse of 150 ms. The magnetic signal was detected in
111 all cases by a compensated pick-up coil system and scaled to low-field magnetization and
112 magnetic susceptibility data.

113 Neutron single-crystal diffraction experiments took place on the E4 and E5 instruments
114 at the BER II reactor of the HZB. We have used a single crystal with dimensions $4 \times 4 \times 4$
115 mm^3 . An incident wavelength $\lambda = 2.4 \text{ \AA}$ was selected with the PG (002) monochromator was
116 utilized in both cases along with a set of $\lambda/2$ filters reducing the contamination of higher-
117 order wavelengths components to a level below 10^{-4} . The E4 diffractometer is equipped
118 with a two-dimensional position sensitive 3He -detector ($200 \times 200 \text{ mm}^2$) enabling an effective
119 mapping and detection of all the available diffracted signals. The superconducting split-pair
120 coil cryomagnet capable of generating magnetic fields up to 14.5 T limited us to ± 2.7 degrees
121 from the scattering plane. The field has been applied along the [001] and [110] directions.

122 In order to determine the crystal structure of U_2Rh_2Sn necessary for analysis of polarized
123 neutron data, we have performed a measurement on a four-circle diffractometer E5 using

124 a shorter neutron incident wavelength of 0.90 Å selected by a Cu monochromator. The
125 E5 instrument is equipped with a two-dimensional position sensitive ^3He -detector (90 x 90
126 mm²).

127 The crystal structure refinements were carried out with the program Xtal 3.4.4²⁴ and the
128 refinements of the magnetic structure have been performed using the program Fullprof (part
129 of the Winplotr suite²⁵). In the refinements, the nuclear scattering lengths $b(\text{Sn}) = 6.23$ fm,
130 $b(\text{Rh}) = 5.88$ fm, and $b(\text{U}) = 8.417$ fm were used²⁶.

131 A polarized neutron diffraction (PND) experiment has been carried out on 5C1 diffrac-
132 tometer installed at the ORPHÉE 14 MW reactor of the Léon Brillouin Laboratory,
133 CEA/CNRS Saclay. Here we have investigated a small (≈ 88 mg) single crystal orig-
134 inating from the same batch as crystals used for other studies. A polarizing Heusler
135 $\text{Cu}_2\text{MnAl}(111)$ monochromator was used to select vertically polarized neutrons with wave-
136 length $\lambda = 0.84$ Å from a hot source. An adiabatic cryoflipper is installed between the
137 monochromator and a vertical superconducting magnet capable to produce 6.2 T. The
138 polarization between different components is maintained using magnetic guides and the
139 resulting incident beam polarization amounts to 88 %.

140 The 5C1 diffractometer is equipped with a large ^3He position sensitive detector covering
141 120 degrees of the scattering angle, 5 degrees below and 18 degrees above the scattering
142 plane. We have collected data at 30 K, i.e. at temperature that is a few K above the
143 magnetic phase transition in two orientations: with the sample's tetragonal axis parallel to
144 the field direction and with field applied perpendicular to it. The magnetic field of 6.2 T
145 has been applied in the former geometry 2 degrees from the c axis, in the latter about 8
146 degrees from the a axis, within the plane perpendicular to the c axis. In both cases we have
147 recorded 270 degrees of samples's rotation and collected over 100 flipping ratios.

148 In the case of the treatment of magnetic intensities (both polarized and unpolarized), we
149 assumed magnetic form factors of the $\text{U}^{3+}/\text{U}^{4+}$ and Rh^{1+} type, respectively²⁸.

150 Using polarized neutron data, magnetic structure factors have been calculated using the
151 Cambridge Crystallography Subroutine Library²⁹ suite programs. Spin densities were recon-
152 structed using the software package PRIMA³⁰ that calculates the most probable distribution
153 that is in agreement with the symmetry of the parent lattice, observed magnetic structure
154 factors and associated errors using the maximum entropy (MAXENT) method³¹. The re-
155 sulting densities were drawn using the computer code VESTA³².

TABLE I. Crystal structure parameters of U_2Rh_2Sn as determined from the neutron data collected at 8 K on E5 using incident wavelength of $\lambda = 0.90 \text{ \AA}$. The thermal parameters U_{ij} (given in 100 \AA^2) are in the form $\exp[-2\pi^2(U_{11} h^2 a^{*2} + 2U_{13} h l a^* c^*)]$, where h, k and l are indices of the relevant Bragg reflection and a^* and c^* are reciprocal lattice constants. For symmetry reasons the values U_{12} (for Sn only), U_{13} and U_{23} of the atoms U, Rh and Sn are equal to zero in this structure. For similar reasons, $U_{11} = U_{22}$ for all the atoms.

U_2Rh_2Sn		Space group: $P4/mbm$				
Atomic positions:			Thermal parameters:			
Atom/Site	x	y	z	U_{11}	U_{33}	U_{12}
U/4h	0.1719(1)	$x + \frac{1}{2}$	$\frac{1}{2}$	0.39(5)	0.55(8)	0.06(4)
Rh/4g	0.3674(2)	$x + \frac{1}{2}$	0	0.39(7)	0.73(8)	-0.06(5)
Sn/2a	0	0	0	0.52(7)	0.5(1)	0
Cell parameters:						
a (\AA)	7.449(1)					
c (\AA)	3.5859(1)					
Agreement factor:			$R_F = 0.073$			

156 III. RESULTS

157 A. Crystal Structure

158 Refined parameters of the X-ray powder pattern are in good agreement with the
 159 literature^{5,6,9,11}. However, additional low-intensity peaks not indexable within the main
 160 structure of U_2Rh_2Sn were detected as well. Since EDX measurements reveal a presence
 161 of a secondary phase with an enhanced uranium content as well, several common uranium
 162 compounds like various carbides and oxides were checked. However, all of them were rejected
 163 in the course of refinement as being the origin of these reflections.

164 Wide-angle diffraction single crystal data collected using E4 diffractometer revealed that
 165 the quality of the crystal was acceptable although it has been found that a minority grain (\approx
 166 6 vol.%) rotated by 1.6 degrees from the main grain exists. Moreover, reflections with $h =$
 167 $2n+1$ not compatible with the space group $P4/mbm$ were observed as well suggesting either

168 a different space group or multiple scattering. The ratio between the 010 and 020 Bragg
169 reflection of 0.15 excludes that these are due to $\lambda/2$ contamination. Although superstructure
170 modifications are not uncommon in this group of compounds³³, a subsequent experiment on
171 E5 diffractometer proved that these reflections are due to multiple scattering.

172 In total 80 individual reflections (29 inequivalent ones) were measured using the E4 diffrac-
173 tometer at several B-T thermodynamic conditions and corrected for the Lorentz factor and
174 extinction which was found to be negligible. The refinement of nuclear reflections collected
175 above the proposed magnetic phase transition temperature in two different orientations
176 lead to crystallographic parameters that are in good agreement with the X-ray data and
177 literature^{5,6}. The agreement factor was $R_F = 0.101$.

178 The appearance of $h00$ reflections with $h = 2n+1$ prompted us to carry out so-called
179 azimuthal ψ -scans around the scattering vector of a reflection in question using the E5
180 diffractometer. It appeared that the intensities of these reflections diminishes at particular
181 positions of ψ , proving a presence of multiple scattering.

182 For the refinement of the crystal structure of U_2Rh_2Sn , we have collected on the E5
183 instrument a data set at 8 K using the incident wavelength $\lambda = 0.90 \text{ \AA}$ 1182 reflections
184 (303 inequivalent ones), all indexable within the space group $P4/mbm$ were used for the
185 refinement. Lattice constants were determined from the orientational UB matrix calculated
186 from 490 Bragg reflections. The fitted parameters are listed in Tab. I.

187 **B. Magnetic bulk properties**

188 In Fig. 2(a) the temperature dependences of the static magnetic susceptibility $\chi = M/H$
189 measured along a and c axis in field of 1 T are shown. Such an approach is valid only in the
190 case where the χ is field-independent up to this field. As it is shown below, the magnetization
191 is (except for a limited temperature range around the magnetic phase transition) linear with
192 field (see Fig. 2). Indeed, values obtained for field of 14 T are only slightly lower.

193 χ is highly anisotropic with the response along the c axis being in the paramagnetic state
194 much larger. This qualifies this direction as the easy magnetization direction. The magnetic
195 susceptibility measured along the $[110]$ direction is identical to that measured along the a
196 axis suggesting that the anisotropy within the basal plane is negligible. With lowering the
197 temperature the response along both a and c axis directions increases. Eventually, both

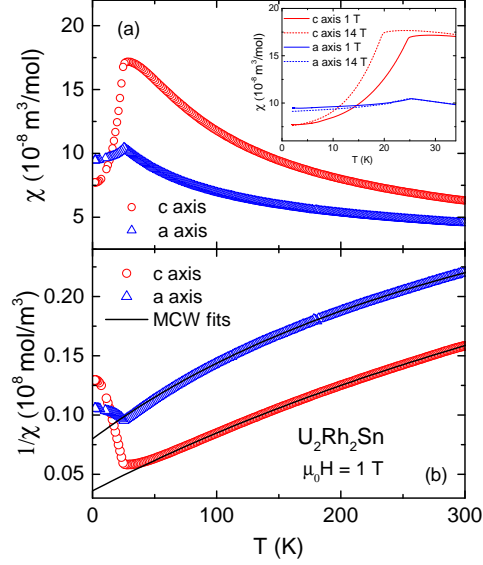


FIG. 2. (Color online) Temperature dependence of the magnetic susceptibility $\chi(T)$ with field applied along the two principal directions (a). The inset magnifies the area around T_N showing also the data taken in 14 T. Panel (b) shows the temperature dependence of the inverse magnetic susceptibility (open points) together with the best fits to a modified Curie-Weiss law (full lines).

198 temperature dependencies exhibit a distinct anomaly at 25 K marking the onset of mag-
 199 netic ordering. Below this temperature new magnetic Bragg reflections appear at positions
 200 suggesting a doubling of the magnetic unit cell with respect to the crystallographic one. The
 201 magnetic ordering is therefore AF and the anomaly can be identified as the Néel temperature.
 202 These findings are in a good agreement with literature data^{8,11,14}. At lower temperatures
 203 a significant drop of χ_c is observed. Notably, both curves cross around 15 K, leading to
 204 a reversed magnetic response at low temperatures. This finding is in a clear contradiction
 205 with previous results by Pereira *et al.* which reports that $\chi_a < \chi_c$ at all temperatures¹¹.

206 In the inset of Fig. 2(a) we show the temperature dependences of the magnetic suscep-
 207 tibilities measured at 1 T and 14 T. As can be seen, the anomaly shifts with magnetic field
 208 applied along the c axis significantly in contrast to the a axis direction where it stays pinned
 209 at 25 K. This corroborates a finding that the c axis direction is in the paramagnetic state
 210 the easy magnetization direction.

211 The magnetic susceptibility along both, the a and the c directions follows at higher tem-
 212 peratures a modified Curie-Weiss (MCW) law according to the expression $\chi_c(T) = \chi_0 +$
 213 $C/(T - \theta_p)$, where χ_0 is temperature independent term, C denotes the Curie constant and
 214 θ_p is the paramagnetic Curie temperature. The best fit to this expression at temperatures
 215 between 70 and 300 K gives an excellent agreement with the experimental data (see the
 216 full lines through the points in Fig. 2(b)). The refined temperature independent term χ_0
 217 amounts to $2.3 \cdot 10^{-8} \text{m}^3/\text{mol}$ and $1.8 \cdot 10^{-8} \text{m}^3/\text{mol}$ for the a and the c axis direction, respec-
 218 tively (both per formula unit). The refined paramagnetic Curie temperatures θ_p amount to
 219 - 84.5(0.2) K and - 62.1(0.1) K for the a and c axis directions, respectively, documenting a
 220 predominantly AF exchange in $\text{U}_2\text{Rh}_2\text{Sn}$.

221 The refined effective moment obtained is 1.65(0.02) μ_B/U and 2.26(0.01) μ_B/U , for the a
 222 and the c axis direction, respectively. These values differ slightly from single crystal values
 223 reported by Perreira *et al.*¹¹ and powder measurements by Havela *et al.*⁸. We attribute the
 224 differences to possible influence of a small misalignment, impurities, fitting method and/or
 225 temperature range in which the magnetic susceptibility was analyzed. Indeed, the best fit
 226 to a Curie-Weiss law performed above 250 K leads an effective moment of 3.2 μ_B/U . This
 227 value is approaching the effective moment of a localized U^{3+} and U^{4+} (3.58 and 3.62 μ_B/U ,
 228 respectively) moment.

229 Magnetization measurements for the a and c axes, M_a and M_c , as a function of applied
 230 static field up to 13 T are shown in Fig.3(a) and (b), respectively. As can be seen, the
 231 magnetization measured along the a axis increases linearly with the applied field and is only
 232 very weakly dependent on the temperature. In contrast, the c axis magnetization that is
 233 linear with field at low temperatures shows in the vicinity of T_N at higher fields a significant
 234 upward curvature. This is very easily seen for the magnetization curve taken at 20 K.
 235 Above ~ 30 K the response along the c axis is again linear. Although M_c is at 2 K and
 236 at all fields up to 13 T lower than the magnetization measured along the a axis it gains at
 237 temperatures above ≈ 15 K values that are larger than M_a . This finding corroborates the
 238 magnetic susceptibility results.

239 Magnetization measurements as a function of applied field up to 58 T taken at 2 K along
 240 the a and the c axes and along the [110] direction, are shown in Fig.4. In agreement with
 241 the low field data, the magnetic response along the a axis ([100]) direction and the [110]
 242 direction remains very similar. Their dependences remain linear with field up to 58 T.

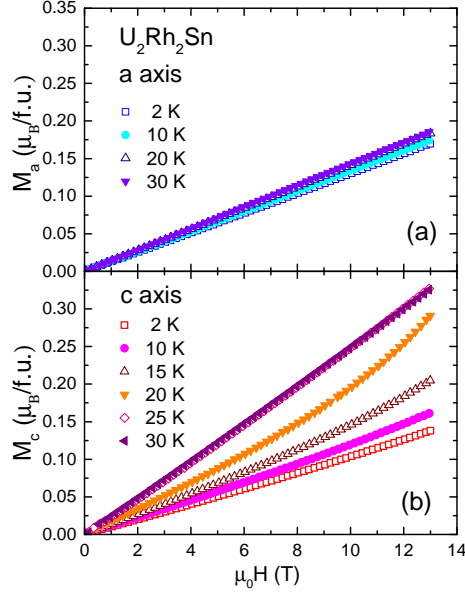


FIG. 3. (Color online) Magnetization measurements as a function of magnetic field applied along the a axis (a) and along the c axis (b) at various temperatures measured using PPMS magnetometer.

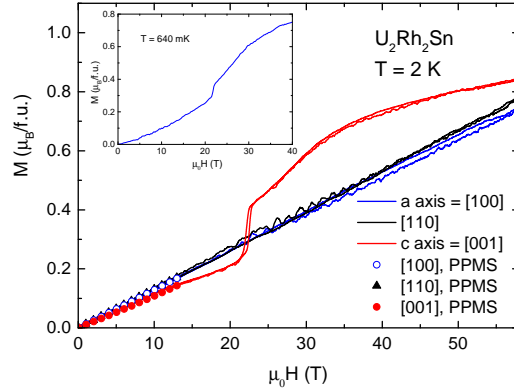


FIG. 4. (Color online) High-field magnetization curves obtained at 2 K in pulse fields applied along the [100], [110] and [001] directions together with the data (shown as full points) taken in static fields using PPMS. In the inset we show the magnetization curve obtained at 640 mK along the c axis using a magnet with a significantly longer pulse duration.

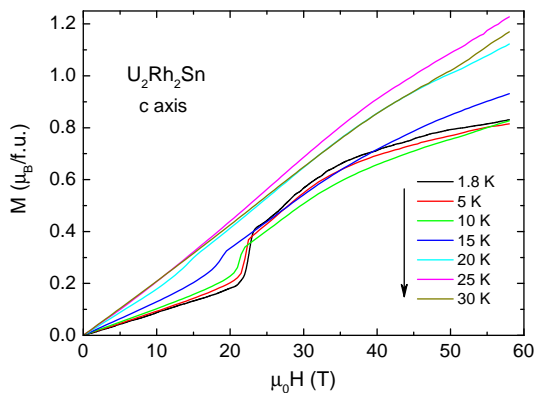


FIG. 5. (Color online) High-field magnetization in increasing pulse fields applied along the c axis direction measured at different temperatures.

243 In contrast, the magnetization measured along the tetragonal axis shows a distinct sharp
 244 metamagnetic transition (MT) located at 22.5 T on the increasing branch and at 22.1 T when
 245 the field is removed. The transition marks a modification of the low-field AF structure. The
 246 magnetization step across the MT amounts only to $0.1 \mu_B/U$ and the magnetization curve
 247 shows at high fields only a very slow tendency towards saturation. The moment attained for
 248 the c axis at 58 T is $0.43 \mu_B/U$. These observations are in agreement with literature data
 249 taken on polycrystalline samples^{17,18}.

250 Above the MT transition the magnetization along the c axis increases monotonically
 251 but not in a trivial way. This observation, suggesting above MT a possible formation of a
 252 plateau similar to SSL materials¹², has prompted us to perform a measurement at 640 mK.
 253 A magnet with a six times longer pulse duration to prevent eddy current heating has been
 254 used. The measured magnetization curve exhibits, however, merely a single MT (see the
 255 inset of 4). We interpret this finding as a consequence of a different duration of the two field
 256 sweeps and a different sensitivity of these measurements to dynamics of the magnetization
 257 process.

258 In Fig.5 we show magnetization curves collected at various temperatures with increasing
 259 magnetic field applied along the c axis up to 58 T. The data have been normalized to
 260 measurements obtained using PPMS. As the temperature increases, the character of the
 261 magnetization process changes significantly. The magnetization step associated with the MT
 262 decreases and the transition itself broadens and shifts to lower fields. The transition can be

263 still discerned in the data taken at 20 K. Simultaneously, the hysteresis of the transition (not
 264 shown) decreases with increasing temperature. Moreover, at low temperatures we observe
 265 a clear tendency towards saturation at high fields. This tendency is weaker above 15 K
 266 and lost at higher temperatures. The magnetization reached at the highest field stays at
 267 low temperatures almost constant but increases with increasing temperature and attains a
 268 maximum at T_N . At the moment it is not clear why the magnetization above T_N is larger
 269 than the saturated value at lower temperatures. One possibility is that dynamical effects
 270 including eddy currents make a reliable scaling to static low field values not possible. Other,
 271 more exotic model suggests that part of the U moment is quenched below the magnetic
 272 phase transition in analogy to URu₂Si₂³. The response along the two remaining directions
 273 is very similar and linear with respect to the applied field up to 58 T at all temperatures
 274 without a sign of any phase transition.

275 C. Specific heat

276 In Fig.6 we show the temperature dependence of the specific heat measured in zero exter-
 277 nal field. A relatively small but a clear anomaly in the temperature dependence of the specific
 278 heat around 25 K can be observed. The specific heat $C(T)$ can be fitted between 2 K and 14
 279 K to a formula $C = \gamma T + \beta T^3$, where γ denotes the electronic low-temperature specific heat
 280 coefficient and β relates to the Debye temperature θ_D via expression $\theta_D^3 = 12\pi^4 R/5\beta$. The
 281 best fit to this formula yields $\gamma = 130.0(0.4)$ mJ / (molK²) and $\theta_D = 168.1(0.7)$ K. These
 282 values are in agreement with literature data⁹. In the upper inset of Fig.6 we present the
 283 experimental data together with the best fit in the C/T vs T^2 representation. In order to be
 284 able to estimate the magnetic entropy connected with the magnetic order a reliable estimate
 285 of the phonon and electronic contributions is needed. We have approximated the phonon
 286 contribution that dominates the specific heat data at temperatures above $T_N = 25$ K using
 287 the Debye specific heat model. The Debye temperature determined from the best fit in the
 288 temperature range 27 - 45 K amounts to $\theta'_D = 184.4(1.1)$ K, a value that agrees reasonably
 289 well with the $\theta_D = 168.1(0.7)$ K from the low-temperature fit. The sum of the electronic
 290 and phonon contributions is shown in the main panel of Fig.6 by a solid line. The difference
 291 with respect to the experimental data can be interpreted as a magnetic specific heat C_{mag} .
 292 Magnetic entropy S_{mag} is obtained by integration of C_{mag}/T . In the lower inset of Fig.6 the

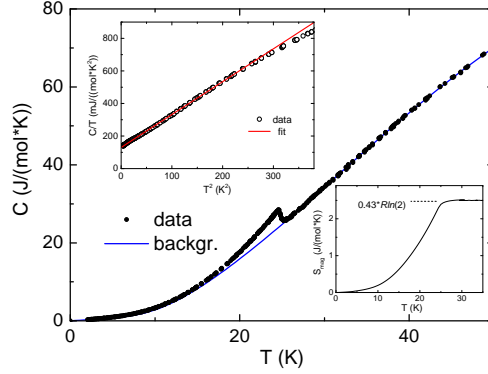


FIG. 6. (Color online) The temperature dependence of the specific heat C of $\text{U}_2\text{Rh}_2\text{Sn}$ single crystal measured in zero magnetic field. The solid line through measured data is the estimation of the phonon background as described in the main text. The lower inset shows the temperature development of the magnetic entropy. The top inset shows the low temperature part of the specific heat in the C/T vs T^2 representation together with the best fit to formula given in the main text.

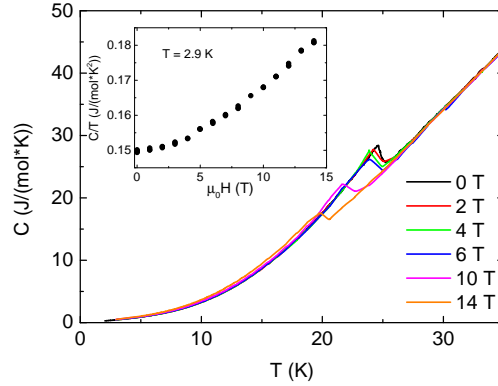


FIG. 7. (Color online) The temperature dependence of the specific heat C of $\text{U}_2\text{Rh}_2\text{Sn}$ single crystal measured in applied magnetic field up to 14 T directed along the tetragonal axis. In the inset we show the variation of the specific heat recorded at 2.9 K with field applied along the c axis.

293 temperature dependence of the $S_{mag}(T)$ documenting that above ≈ 25 K S_{mag} approaches
 294 a value of $0.43 R \ln(2)$, i.e. a value that is significantly smaller than a value expected for
 295 fully developed U magnetic moments, however, in agreement with literature^{1,9}. Note that
 296 the S_{mag} is determined per two U atoms.

297 In Fig.7 we show the temperature dependence of the $\text{U}_2\text{Rh}_2\text{Sn}$ specific heat measured

298 in zero external field and in fields up to 14 T applied along the tetragonal axis. The
 299 anomaly gets somewhat smeared out with increasing the applied field and shifts towards
 300 lower temperatures. The magnetic entropy obtained by integration of C_{mag}/T up to 30 K,
 301 i.e. in the same temperature range, does not change substantially as a function of applied
 302 field and remains nearly constant. This suggests that the magnetic entropy shifts merely
 303 to lower temperatures. Indeed, the isothermal specific heat increases at low temperatures
 304 slightly as a function of field. This is documented in the inset of Fig.7, where we show the
 305 specific heat measured at 2.9 K divided by the temperature as a function of the applied
 306 field.

307 **D. Electrical resistivity**

308 In Fig.8 we show the electrical resistivity measured along the c axis in the temperature
 309 range between 2 and 300 K. The electrical resistivity is rather large at high temperatures
 310 (at 300 K, ρ_c , attains $127 \mu\Omega\text{cm}$) and increases slightly upon cooling. It exhibits a broad
 311 maximum around 200 K and falls down strongly below 70 K. It shows an anomaly in the
 312 resistivity data at 25 K as shown in the inset of Fig.8 that is connected with AF ordering and
 313 levels-off in the low-temperature limit. These results are in good agreement with literature
 314 data^{9,16}.

315 The low-temperature part that is shown in the inset of Fig.8 cannot be described by an
 316 ordinary Fermi-liquid dependence of the form $\rho(T) = \rho_0 + aT^n$ with $n = 2.0$. The best
 317 fit to data between 2 and 15 K yields $n = 2.29(1)$. However, even better agreement with
 318 data in the same temperature range is obtained for expression $\rho(T) = \rho_0 + aT^2 + bT(1 +$
 319 $2T/\Delta)e^{-\Delta/T}$ yielding $\rho_0 = 27.5(2) \mu\Omega\text{cm}$, $a = 0.025(8) \mu\Omega\text{cmK}^{-2}$, $b = 0.59(2) \mu\Omega\text{cmK}^{-1}$
 320 and $\Delta = 7.7(1.7)$ K. The fit is shown in Fig.8 by the solid line through the experimental
 321 points. This formula has been introduced in order to account for the influence of an energy
 322 gap Δ in the dispersion relation of magnetic excitations caused by strong electron-magnon
 323 coupling³⁴.

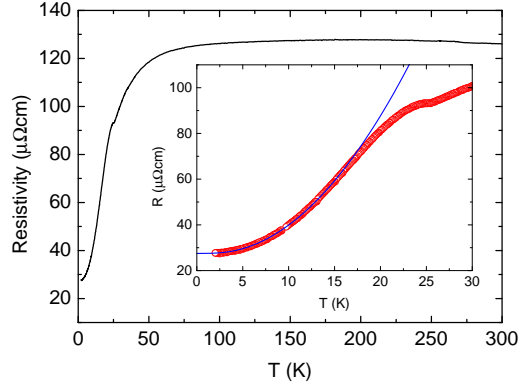


FIG. 8. (Color online) Electrical resistivity of U_2Rh_2Sn single crystal measured along the c axis. The inset shows the low-temperature detail of the electrical resistivity curve to focus on the anomaly caused by the onset of antiferromagnetism and the best fit to the expression described in the main text.

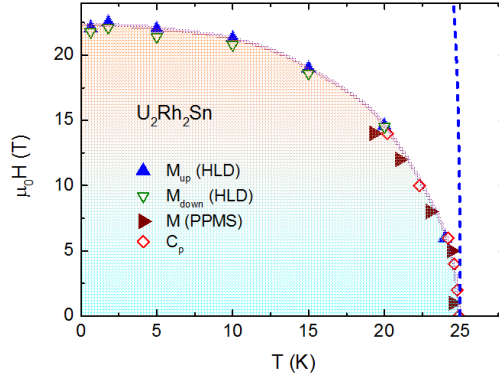


FIG. 9. (Color online) Magnetic phase diagram of U_2Rh_2Sn for field applied along the c axis determined from high field pulse measurements (HLD) and magnetization and specific heat measurements using static fields. The magnetic phase diagram for field applied along the a axis is shown schematically by the broken, nearly vertical line.

324 E. Magnetic phase diagram

325 Combining all the available experimental data allowed for construction of the magnetic
 326 phase diagram as shown in Fig.9. All the measurements show that the magnetic field alters
 327 the magnetic order in U_2Rh_2Sn in a step-like manner only if it is applied along the tetragonal

axis. This is documented by the invariance of the magnetic phase transition temperature $T_N = 25$ K and absence of any field-induced transition for field applied within the ab plane up to 58 T. For the a axis we observe that the $T_N = 25$ K is independent of field at least up to 14 T. For higher fields only measurements up to 58 T at constant temperatures are available leading to a conclusion that the low-field phase is not altered up to this field applied along the a axis. On the contrary, for the c axis we observe significant modifications.

Such a magnetic phase diagram is very similar to many other U-based compounds showing strong magnetocrystalline anisotropy¹. In particular, it documents robustness of the magnetic order against the magnetic field applied perpendicular to the c axis. Such a behavior is conventionally explained by the direct $5f$ - $5f$ electron wave-functions overlap and their hybridization with ligand states that locks U moments along a specific direction^{1,9}.

F. Magnetic Structure

As the temperature is lowered below the magnetic phase transition temperature $T_N = 25$ K, new Bragg reflections appear at positions indexable with a single propagation vector $\mathbf{k} = (0, 0, \frac{1}{2})$. This observation proves the existence of an AF order. In Fig.10 we show a representative scan through the $(1\ 1\ \frac{1}{2})$ magnetic Bragg reflection taken at 2 K and at 26 K in zero field and at 2.4 K in a field of 14.5 T applied along the $[\bar{1}\ 1\ 0]$ direction. As it can be seen, the intensity of this reflection vanishes above T_N . No intensities are observed at any $(0\ 0\ \frac{l}{2})$, reciprocal space positions. These findings are entirely in agreement with the literature^{9,11,35}. In total we have collected on the E4 diffractometer a set of 36 magnetic reflections (18 unique ones) at various positions within the magnetic phase diagram. For the refinement of the AF structure we have used a data set taken at 2.4 K in zero field. To obtain the magnetic moment values we have used the structural parameters as described above and initially assumed that only U atoms carry magnetic moment.

In order to refine the magnetic structure one conventionally compares intensity of magnetic reflections calculated from all possible magnetic structure models that are compatible with the observed magnetic propagation vector and the paramagnetic space group. These models are deduced by using a symmetry group analysis as developed by Bertaut³⁶. Analysis for the propagation vector $\mathbf{k} = (0, 0, \frac{1}{2})$, site $4h$ and the space group $P4/mbm$ has been performed earlier and is available in the literature^{19,35}. U moments are confined either

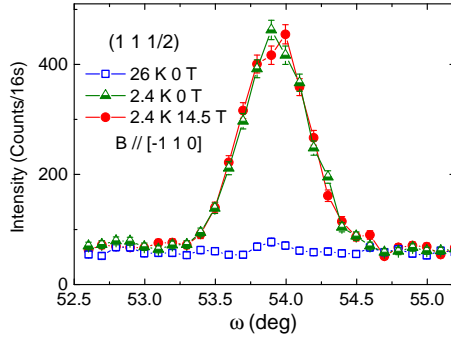


FIG. 10. (Color online) Rocking curves through the $(1\ 1\ \frac{1}{2})$ magnetic Bragg reflection collected at 2.4 K and at 26 K (just above the magnetic phase transition) in zero field and at 2.4 K in a field of 14.5 T applied along the $[\bar{1}\ 1\ 0]$ direction.

358 within the basal plane or oriented in a collinear fashion along the c axis.

359 After testing all possibilities it became clear that only the model shown in Fig.11a (in
 360 the original paper of Bourée *et al.*³⁵ as Γ_8) can explain the observed intensities satisfactorily.
 361 This model leads agreement to factors that are at least two or three times lower than for
 362 other models. The refined moment amounts to $0.55(1)\ \mu_B/U$ and the agreement factor
 363 was $R_M = 0.051$. The moment value resulting from this fit is larger than result obtained
 364 on powder sample⁹ and in good agreement with the moment obtained by Pereira *et al.*¹¹.
 365 Nevertheless, as magnetic moments on Rh sites cannot be excluded, we have performed
 366 the symmetry group analysis also for the $4g$ site taken by Rh atoms. The analysis leads for
 367 moments at the Rh $4g$ sites to very similar magnetic moment configurations as in the case of
 368 U moments at $4h$ sites. Rh moments are either confined to the basal plane or directed along
 369 the c axis. However, in many cases their directions are within one irreducible representation
 370 (irrep) perpendicular to U moments. In particular, in the case of the model associated with
 371 irrep Γ_8 described above are the Rh moments confined to the ab plane, in the case of Γ_3 ,
 372 reported for U_2Ni_2In are the U moments in plane but Ni moments along the c direction^{9,19}.
 373 The best agreement is found for Γ_8 with U moments of $0.50(2)\ \mu_B$ (along the c axis) and
 374 Rh moments of $0.06(4)\ \mu_B$ (within the ab plane). The resulting AF structure is shown in
 375 Fig.11b. The agreement factor improved slightly to $R_M = 0.045$ with χ^2 dropping by few %
 376 as well. However, the refined Rh moments are very small and at the limit of the sensitivity
 377 of our unpolarized neutron diffraction experiment. The sensitivity to small moments can be

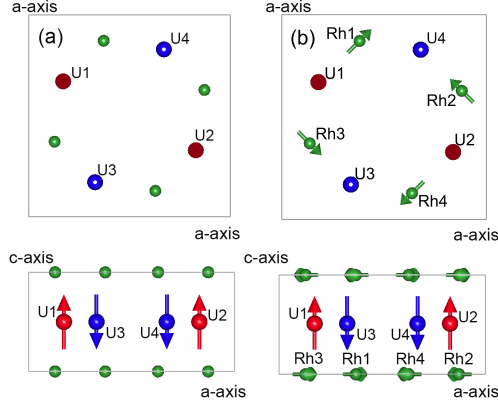


FIG. 11. (Color online) Schematic representation of the AF structure of U_2Rh_2Sn as determined from the best fit of our neutron diffraction data taken at 2.4 K in zero external field to the model assuming the existence of only U moments (a). AF structure of U_2Rh_2Sn assuming the existence of both, U and Rh moments is shown in (b). Rh moments were multiplied by a factor of five. Both structures are shown in two projections: along the tetragonal axis (top) and along the a axis (lower panel). Only half one magnetic unit cells are shown. Moment directions in the adjacent cells along the c axis are reversed.

378 improved in a polarized neutrons experiment that is described below.

379 In Figs.2 and 10 we demonstrate also the robustness of the magnetic structure against the
 380 influence of the magnetic field applied at low temperature both along and perpendicular to
 381 the tetragonal axis. The intensities of nuclear reflections are not influenced up to the highest
 382 magnetic field of 14.5 T available with the superconducting magnet applied along the c axis.
 383 For this geometry we could not observe any magnetic reflections. If the magnetic structure
 384 would be alternated, there would be a small increase of intensities due to a ferromagnetic
 385 component visible on top of e.g. 110 and 200 reflections. In the present experiment with
 386 field applied along the c axis we can conclude that the induced moment is less than ≈ 0.1
 387 μ_B/U at 14.5 T and 2 K.

388 In Fig.12 we demonstrate that magnetic reflections are also not influenced at low tem-
 389 peratures if the field is applied along the $[\bar{1} 1 0]$ direction. A sizable effect for this field
 390 orientation can be seen only in a very close vicinity of T_N . This is documented in Fig. 12
 391 which shows the temperature dependence of the $(1 1 \frac{1}{2})$ magnetic reflection measured with
 392 increasing temperature in zero field and in a field of 14.5 T. The intensity of this reflection
 393 continuously decreases with increasing temperature and vanishes around $T_N = 25$ K. There

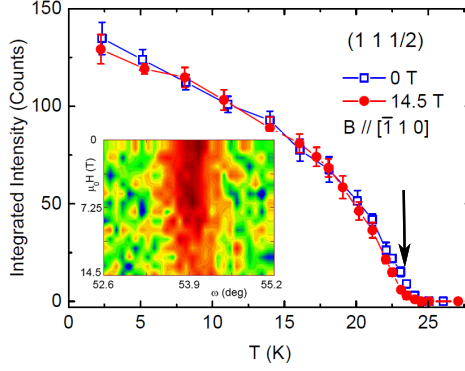


FIG. 12. (Color online) Temperature dependence of the $(1\ 1\ \frac{1}{2})$ magnetic Bragg reflection recorded with increasing temperature in zero field and in field of 14.5 T applied along the $[\bar{1}\ 1\ 0]$ direction. The arrow in the main panel denotes conditions under which a field scan shown as a color coded map (shown in the inset) of intensities taken at the same reflection has been taken with decreasing field.

394 is a tiny shift negative in T_N and difference in the intensity of the reflection when a field is
 395 applied. An isothermal field scan taken at 23 K with decreasing field is shown in the form of
 396 color coded map in the inset of Fig. 12. It shows that the intensity of the $(1\ 1\ \frac{1}{2})$ magnetic
 397 reflection increases upon removal of the field. However, the increase is very tiny. Assuming
 398 that the magnetic structure remains stable up to T_N , the moment change between 14.5 T
 399 and zero field could be estimated to be less than $0.12\ \mu_B/U$.

400 G. Polarized Neutrons

401 The use of a polarized neutron beam is known to be very beneficial for observation of small
 402 field-induced magnetic moments. In the case of small ferromagnetic component that appear
 403 at the top of nuclear Bragg reflections is this method (based on the interference between
 404 nuclear and magnetic contributions) especially indispensable³⁷. In order to be able extract
 405 the magnetic structure factors used in further refinement, one has to use reliable crystallo-
 406 graphic information. In our case we have determined the crystal structure of U_2Rh_2Sn to
 407 a great precision at 8 K, at a not very different temperature at which polarized neutron
 408 experiment has been performed. The magnetic structure factors have been obtained from
 409 a data set collected at 30 K using crystallographic data listed in Table I above. Twenty

410 six flipping ratios with a signal larger than one statistical deviation have been used in the
 411 analysis. However, it has to be noted that all the flipping ratios are close to unity and
 412 the fits to atomic models (with or without allowing Rh moments) are very unstable. It is
 413 therefore difficult to discriminate between different models. Another approach, a maximum
 414 entropy reconstruction³¹, does not rely on any particular atomic model and yield the most
 415 probable spin density distribution compatible with experimental data and the underlying
 416 lattice symmetry.

417 In Fig. 13 we show such spin distributions reconstructed using this method. Two different
 418 significant magnetization clouds can be identified. One is situated in the vicinity of U atoms
 419 and the other, much smaller, in the vicinity of Rh atoms. The shift of the density maxima
 420 from atomic positions is in both cases small. Integration around these positions using
 421 relevant ionic radii³⁸ lead to magnetic moments of $\sim 0.02 \mu_B$ at the U site and slightly less
 422 than $\sim 0.01 \mu_B$ at Rh positions. The total magnetic moment associated with all the U
 423 and Rh sites in the unit cell amounts to $\sim 0.12 \mu_B$, a value that should be compared with
 424 the magnetization value of $0.16 \mu_B$ obtained from the magnetization measurements. The
 425 difference is attributed to a conduction-electron polarization.

426 A rather important result of this analysis is a significant polarization associated with
 427 Rh sites. Such an observation that has been previously made in the case of other U-based
 428 compounds^{1,20,21,39,41} is understood in terms of an anisotropic $5f-d$ hybridization. However,
 429 the moment found on the transition metal atom is usually about one order of magnitude
 430 smaller than the leading magnetic moment associated with $5f$ states. For instance, a detailed
 431 study on a paramagnetic U_2Co_2Sn adopting the same crystal structure⁴⁰ show U magnetic
 432 moments of $0.118 \mu_B$ and Co moments of only $0.013 \mu_B$. In the case of U_2Rh_2Sn , however,
 433 we find that the Rh moment is only slightly less than a half of that at uranium. This seems
 434 to be not very compatible with the generally accepted picture regarding the hybridization-
 435 induced moment mechanism. On the other hand, it should be noted that our unpolarized
 436 neutron study indicated at low temperatures also a possible Rh moment. Furthermore, a
 437 similar study on isostructural U_2Ni_2In ⁹ suggested a significant moment residing at Ni sites
 438 attaining more than 60 % of the uranium moment as well.

439 Unfortunately, the results of the measurement with the field perpendicular to the c axis
 440 are more uncertain. On one hand the spin distribution map shows well the clouds that can
 441 be associated with U and Rh sites. On the other it exhibits many noisy maxima that have

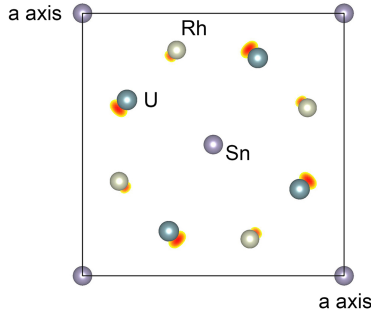


FIG. 13. (Color online) Projection of the spin distribution in U_2Rh_2Sn onto a plane perpendicular to the c axis as obtained from the maximum entropy reconstruction from data collected at 30 K with a field of 6.2 T applied along the tetragonal axis. Only half of the unit cell along the c direction is projected. Densities around magnetic moments are restricted by an isosurface value of $0.01 \mu_B/\text{\AA}^3$. Densities below this level are not shown.

442 no relation with any other atomic positions. We attribute this to the fact that the magnetic
 443 susceptibility along this direction is smaller than along the c axis and also the symmetry is
 444 reduced from the tetragonal one by the applied field. A much larger crystal is needed to
 445 perform a reliable experiment along this direction. The same holds also for measurement at
 446 low temperatures where the magnetic susceptibility along the c axis drops significantly.

447 IV. DISCUSSION AND CONCLUSIONS

448 In this work we have investigated in detail the magnetic, thermal and electrical transport
 449 properties of the intermetallic compound U_2Rh_2Sn using variety of experimental techniques
 450 and determined its crystallographic and AF structures.

451 In agreement with literature, we have found that this system orders below $T_N = 25$ K. The
 452 AF phase transition is manifested in temperature dependences of the magnetic susceptibility,
 453 the specific heat, electrical resistivity and by an appearance of magnetic reflections indexable
 454 with $\mathbf{k} = (0, 0, \frac{1}{2})$. The magnetic entropy associated with the magnetic order is small and
 455 attains only a fraction of the value expected for a fully developed U moment. This suggests
 456 highly reduced U magnetic moment values. Indeed, U moments of 0.50 - 0.55 μ_B at 2.4 K
 457 were detected, Rh moments being even smaller. Such U value is greatly reduced with respect
 458 to U^{3+} or U^{4+} free ion values and suggests that the magnetism in U_2Rh_2Sn is governed by

459 hybridization effects which induce Rh moments that are in the low-temperature limit about
 460 ten times smaller than at U sites. These results in turn agree with the best fits to a modified
 461 Curie-Weiss law. These show a strongly reduced effective magnetic moment, a signature of
 462 non-localized magnetic moments. The localization is found only at high temperatures.

463 The easy magnetization direction in the paramagnetic state is found to be along the
 464 tetragonal axis with a negligible anisotropy within the ab plane that is the hard magne-
 465 tization direction. However, in contrast to previous studies we observe that the c axis is
 466 the easy magnetization axis only close and above the magnetic phase transition. At lower
 467 temperatures the response perpendicular to the c axis becomes stronger. Normally, a differ-
 468 ent behavior of perpendicular χ_{\perp} and longitudinal χ_{\parallel} magnetic susceptibility in a classical
 469 antiferromagnet can be explained by the fact that it is easier to tilt magnetic moments by
 470 the field than to increase their magnitudes, i.e. one expects $\chi_{\perp} > \chi_{\parallel}$ below T_N . This is not
 471 the case of uniaxial U-based systems where the anisotropy energy is so strong that any tilt
 472 from the unique axis is impossible leading to $\chi_{\perp} < \chi_{\parallel}$ at all temperatures¹. In the present
 473 system the $\chi_{\parallel} = \chi_c$ is larger than χ_{\perp} only in the vicinity and above the T_N but smaller in
 474 the low temperature region.

475 Neutron diffraction experiments proved that the magnetism in U_2Rh_2Sn is associated
 476 mainly with $5f$ states. However, a significant contribution originating from Rh electronic
 477 states is found as well. The observed magnetic structure might account for the peculiar
 478 temperature dependence of the magnetic susceptibility. Comparing the zero field unpolar-
 479 ized neutron results at 2.4 K with polarized data obtained above the T_N we conclude that
 480 U and Rh sites might contribute to the magnetic susceptibility at different temperatures
 481 differently. At low temperatures are U moments of $0.50(2) \mu_B$ oriented along the c axis and
 482 can contribute to χ_c only via changing their magnitude. Strong anisotropy does not allow
 483 them to be tilted from the c axis direction significantly. Still, $\chi_{\perp} > \chi_{\parallel}$ is observed. The
 484 Rh moments that are about ten times smaller are confined in a non-linear fashion to the
 485 basal plane due to a necessity to belong to the same irrep. They can thus contribute both
 486 to the χ_c and χ_{ab} by their tilting away from the $[110]$ type planes. We therefore attribute
 487 the peculiar behavior of $\chi(T)$ at low temperatures to the existence of Rh moments.

488 The above mentioned explanation of the susceptibility behavior relies on the assumption
 489 that the U moment sublattice in U_2Rh_2Sn exhibits inherently an uniaxial type of anisotropy
 490 that does not change with temperature. However, a generally accepted hybridization-

491 induced anisotropy considers all contributions to an anisotropic hybridization and the direct
 492 $5f$ - $5f$ wave function overlap. As the hybridization increases with shortening the interatomic
 493 distances, it is expected that the contribution from the latter mechanism would lead to U
 494 moments that lie within the basal plane. The $5f$ - d hybridization would support this configu-
 495 ration as well because the Rh atoms lie outside the U-basal plane (see Fig.1(a)). Apparently,
 496 the experiment shows that U moments orient along the c axis. It should be, however, men-
 497 tioned that for each U atom there is one next-nearest (NN) U neighbor and further four
 498 second-next-nearest (SNN) U neighbors at distances that are only 1.00 % and 8.81 % larger
 499 than the nearest neighbors found along the c axis. A competition between in-plane and
 500 out-of plane can be thus expected.

501 As mentioned above, both, Rh and U sublattices in U_2Rh_2Sn map onto an effective 3D
 502 Shastry-Sutherland lattice. It is interesting to note that, considering only U moments, the
 503 observed AF structure belongs to one of the possible magnetic structures in zero magnetic
 504 field realized in an Ising system - the so-called Néel state¹². The NN U moments at a distance
 505 of d_1 (exchange J in Fig. 1(c)) are coupled ferromagnetically (thus, $J > 0$) and do not form
 506 within the ab plane AF dimers. On the contrary, all couplings between SNN U neighbors
 507 are AF ($J' < 0$). Such a coupling would indicate $|J| < |J'|$. For comparison, in TmB_4
 508 and TbB_4 , where $4f$ moments lie within the basal plane, the $J < 0$ and $|J| > |J'|$ ^{13,42}.
 509 A further difference is that the coupling along the c axis is in U_2Rh_2Sn AF and in TmB_4
 510 ferromagnetic. The situation within the Rh magnetic sublattice is more complex as they are
 511 non-collinear.

512 The high-field magnetization experiments in pulse fields up to 58 T with field applied
 513 along the $a = [100]$, $[110]$ and $c = [001]$ directions were performed. The MT seen for
 514 the c axis shifts with increasing temperature towards lower fields. The response along the
 515 two remaining directions is very similar and linear with respect to the applied field up to
 516 58 T at all temperatures without a signature of a phase transition. A magnetic phase
 517 diagram has been constructed. The magnetization attained at low temperatures at the
 518 highest field applied along the c axis of $0.43 \mu_B/U$ is to be compared with the neutron
 519 value found for the zero-field AF state. The discrepancy along with a rather large high-field
 520 magnetic susceptibility without a clear saturation at even 58 T suggests that U moments
 521 are stabilized by the magnetic field. A complex magnetization curve for the field applied
 522 along the tetragonal axis suggests that the magnetization process is not of a simple spin-flip

523 type. It is to expected that a contribution from Rh moments that make at low temperatures
524 a complicated non-collinear arrangement similar to SSL lattice system, plays an important
525 role. However, a search for possible magnetic states with fractionalized magnetization values
526 (as observed in TmB_4 ⁴² or $\text{SrCu}_2(\text{BO}_3)_2$ ⁴³) was not successful. Nevertheless, in the view of
527 the high critical field applied along the tetragonal axis necessary to destroy the ground-state
528 AF structure of 22.5 T and create presumably only partially ferromagnetically aligned U and
529 Rh moments it would be interesting to perform a high-field neutron diffraction experiment
530 using the 26 T HFM-EXED facility⁴⁴.

531 ACKNOWLEDGMENTS

532 We acknowledge the support of the HLD at HZDR, member of the European Magnetic
533 Field Laboratory (EMFL). We acknowledge also allocated beam time at the laboratoire Léon
534 Brillouin Saclay and technical support received. Experiments were performed partially in
535 MLTL (<http://mltl.eu/>) which is supported within the program of Czech Research Infras-
536 tructures (project no. LM2011025). This work was also supported in part by the project
537 16-03593S of the Czech Science Foundation. We would like to thank R. Wimpory from HZB
538 for checking our manuscript.

539 * prokes@helmholtz-berlin.de

540 ¹ V. Sechovský and L. Havela, *Handbook of Magnetic Materials* Vol. 11 ed. K. H. J. Buschow
541 (North Holland, Amsterdam) pp. 1-289.

542 ² T. T. M. Palstra, A. A. Menovsky, J. van den Berg, A. J. Dirkmaat, P. H. Kes, G. J. Nieuwen-
543 huys, J. A. Mydosh, *Phys. Rev. Lett.* **55**, 2727 (1985).

544 ³ J. A. Mydosh and P. M. Oppeneer, *Rev. Mod. Phys.* **83**, 1301 (2011).

545 ⁴ D. Aoki, A. Huxley, E. Ressouche, D. Braithwaite, J. Flouquet, J. P. Brison, E. Lhotel and C.
546 Paulsen, *Nature* **413**, 613 (2001).

547 ⁵ M. N. Peron, Y. Kergadallan, J. Rebizant, D. Meyer, S. Zwirner, L. Havela, H. Nakotte, J. C.
548 Spirlet, G. M. Kalvius, E. Colineau, J. L. Oddou, C. Jeandey, J. P. Sanchez and J. M. Winand,
549 *J. Alloys Compd.* **201**, 203 (1993).

- 550 ⁶ F. Mirambet, P. Gravereau, B. Chevalier, L. Trut and J. Etourneau, *J. Alloys Compd.* **191**, L1
551 (1993).
- 552 ⁷ H. Nakotte, K. Prokeš, E. Brück, N. Tang, F. R. de Boer, P. Svoboda, V. Sechovský, L. Havela,
553 J. M. Winand, A. Seret, J. Rebizant and J. C. Spirlet, *Physica B* **201**, 247 (1994).
- 554 ⁸ L. Havela, V. Sechovský, P. Svoboda, H. Nakotte, K. Prokeš, F. R. de Boer, A.
555 Seret, J. M. Winand, J. Rebizant, J. Spirlet, A. Purwanto and R. A. Robinson,
556 *J. Magn. Magn. Mater.* **140 – 144**, 1367 (1995).
- 557 ⁹ H. Nakotte, A. Purwanto, R. A. Robinson, K. Prokeš, J. C. P. Klaasse, P. F. de Châtel, F. R.
558 de Boer, L. Havela, V. Sechovský, L. C. J. Pereira, A. Seret, J. Rebizant, J. C. Spirlet and F.
559 Trouw, *Phys. Rev. B* **53**, 3263 (1996).
- 560 ¹⁰ V. Sechovský, L. Havela, H. Nakotte, F. R. de Boer and E. Brück, *J. Alloys Compd.* **138**, 307
561 (1994).
- 562 ¹¹ L. C. J. Pereira, J. A. Paixão, P. Estrela, M. Godinho, F. Boudarot, M. Bonnet, J. Rebizant,
563 J. C. Spirlet, and M. Almeida, *J. Phys. : Condens. Matter* **8**, 11167 (1996).
- 564 ¹² B. S. Shastry and B. Sutherland, *Physica B* **108**, 1069 (1981).
- 565 ¹³ T. Matsumura, D. Okuyama, and Y. Murakami, *J. Phys. Soc. Jpn.* **76**, 015001 (2007).
- 566 ¹⁴ V.H. Tran, Z. Zolnierek, A. J. Zaleski and H. Noël, *Solid State Comm.* **101**, 709 (1997).
- 567 ¹⁵ L. Havela, , V. Sechovský, P. Svoboda, M. Diviš, H. Nakotte, K. Prokeš, F. R. de Boer, A.
568 Purwanto, R. A. Robinson, A. Seret, J. M. Winand, J. Rebizant, J. C. Spirlet, M. Richter, and
569 H. Eschrig, *J. Appl. Phys.* **76**, 6214 (1994).
- 570 ¹⁶ A. M. Strydom, P. de V. du Plessis and V. V. Gridin, *Physica B* **225**, 89 (1996).
- 571 ¹⁷ F. R. de Boer, K. Kindo, H. Nakotte, K. Prokeš and V. Sechovský,
572 *Physica B : Cond. Mat.* **246 – 247**, 129 (1998).
- 573 ¹⁸ T. Fukushima, S. Matsuyama, T. Kumada, K. Kindo, K. Prokeš, H. Nakotte, F. R. de Boer, L.
574 Havela, V. Sechovský, J. M. Winand, J. Rebizant and J. C. Spirlet, *Physica B* **211**, 142 (1995).
- 575 ¹⁹ F. Bourée, B. Chevalier, L. Fournés, F. Mirambet, T. Roisnel, V. H. Tran and Z. Zolnierek,
576 *J. Magn. Magn. Mater.* **138**, 307 (1994).
- 577 ²⁰ J. A. Paixão, G. H. Lander, P. J. Brown , H. Nakotte, F. R. de Boer and E. Brück,
578 *J. Phys. : Condens. Matter* **4**, 829 (1992).
- 579 ²¹ P. Javorský, V. Sechovský, J. Schweizer, F. Bourdarot, E. Lelièvre-Berna, A. V. Andreev and
580 Y. Shiokawa, *Phys. Rev. B* **63**, 064423 (2001).

- 581 ²² Y. Haga, T. Honma, E. Yamamoto, H. Ohkuni, Y. Onuki, M. Ito, and N. Kimura,
582 *Jpn.J.Appl.Phys.* **37** 3604 (1998).
- 583 ²³ V. Petříček, M. Dušek and L. Palatinus, Jana2006. The crystallographic computing system.
584 Institute of Physics, Praha, Czech Republic (2006).
- 585 ²⁴ S. R. Hall, G. S. D. King, J. M. Stewart, Eds., Xtal3.4 Users Manual. University of Australia:
586 Lamb, Perth (1995).
- 587 ²⁵ T. Roisnel and J. Rodríguez-Carvajal, *Mat. Sci. Forum* **378**, 118 (2001).
- 588 ²⁶ V. F. Sears, in: *Int. Tab. for Crystallogr., vol. C*, ed. A.J.C. Wilson (Kluwer Academic Pub-
589 lisher, Dordrecht/Boston/London, 1995), Vol. C., p. 383.
- 590 ²⁷ A. J. Freeman, J. P. Desclaux, G. H. Lander, and J. Faber, Jr., *Phys. Rev. B* **13**, 1168 (1976).
- 591 ²⁸ G. H. Lander, M. S. S. Brooks, and B. Johansson, *Phys. Rev. B* **43**, 13672 (1991).
- 592 ²⁹ P. J. Brown and J. C. Matthewman, The Cambridge Crystallography Subroutine Library, Mark
593 4 Users Manual, Rutherford Appleton Laboratory Report, (1993).
- 594 ³⁰ F. Izumi, R.A. Dilanian, in: *Recent Research Developments in Physics, Part II*, (3Transworld
595 Research Network, Trivandrum 2002) p. 699
- 596 ³¹ J. Skilling and S. F. Gull, in: *Maximum Entropy and Bayesian Methods in Inverse Problems*,
597 eds C. Ray Smith and W. T. Grandy, Jr. (D. Reidel Publishing Comp., Dordrecht, 1985), p. 83.
- 598 ³² K. Momma and F. Izumi, *J. Appl. Crystallogr.*, **44**, 1272 (2011).
- 599 ³³ K. Prokeš, P. Svoboda, A. Kolomiets, V. Sechovský, H. Nakotte, F. R. de Boer, J. M. Winand,
600 J. Rebizant and J. C. Spirlet *J. Magn. Magn. Mater.* **202**, 451 (1999) 451.
- 601 ³⁴ N. H. Andersen and H. Smith, *Phys. Rev. B* **19**, 384 (1979).
- 602 ³⁵ J. Rodríguez-Carvajal and F. Bourée, *EPJ Web of Conferences* **22**, 00010 (2012).
- 603 ³⁶ E. F. Bertaut, *J. Magn. Magn. Mater.* **24**, 267 (1981).
- 604 ³⁷ B. M. T. Willis, *Thermal Neutron Diffraction* (Oxford University Press, Oxford) p. 190.
- 605 ³⁸ R. D. Shannon, *Acta Crystallogr.*, **A32**, 751 (1976).
- 606 ³⁹ K. Prokeš and A. Gukasov, *Phys. Rev. B* **79**, 024406 (2009).
- 607 ⁴⁰ J. A. Paixão, L. C. J. Pereira, P. Estrela, M. Godinho, M. Almeida, L. Paolasini, M. Bonnet,
608 J. Rebizant and J. C. Spirlet *J. Phys. : Condens. Matter* **11**, 2115 (1999).
- 609 ⁴¹ K. Prokeš, A. de Visser, Y. K. Huang, B. Fak, and E. Ressouche *Phys. Rev. B* **81**, 180407(R)
610 (2010).

- 611 ⁴² K. Siemensmeyer, E. Wulf, H.-J. Mikeska, K. Flachbart, S. Gabani, S. Matáš, P. Priputen, A.
612 Efdokimova and N. Shitsevalova, *Phys. Rev. Lett.* **101**, 177201 (2008).
- 613 ⁴³ Y. H. Matsuda, N. Abe, S. Takeyama, H. Kageyama, P. Corboz, A. Honecker, S. R. Manmana,
614 G. R. Foltin, K. P. Schmidt and F. Mila, *Phys. Rev. Lett.* **111**, 137204 (2013).
- 615 ⁴⁴ P. Smeibidl, A. Tennant, H. Ehmler and M. Bird *J. Low. Temp. Phys.* **159**, 402 (2010).